JOURNAL OF SOLID STATE CHEMISTRY 95, 319–326 (1991)

# Crystal Structure of Polymeric Pyrite Type $Ir_3Te_8$

STÉPHANE JOBIC, MICHEL EVAIN, RAYMOND BREC,*
PHILIPPE DENIARD, ALAIN JOUANNEAUX, AND JEAN ROUXEL

*Laboratoire de Chimie des Solides, U.M. 110, IMN, 2 rue de la Houssinière, 44072, Nantes Cédex 03, France*

Received February 18, 1991

A single crystal X-ray diffraction study performed on pyrite-like $Ir_3Te_8$ indicates that this compound has rhombohedral symmetry. Magnetic measurements were performed to determine the formal 3+ oxidation state of Ir. This value aided in explaining the interatomic distances of our structure determination. $Ir_3Te_8$ has been found to belong to a polymeric-type structure, with a tridimensional network made of interlinked $Te_2$ pairs. The results are compared with pyrite-like $MTe_2$ ($M$ = Mn, Fe, Ni, Cu, Ru, Rh, and Os). 

## I. Introduction

Previous investigations (*1*, *2*) on the Ir–chalcogen phases have shown that they present various anionic oxidation states. In the iridium dichalcogenides $IrX_2$, with $X$ = S and Se, the charge balance formulation can be written $Ir^{3+}X^{-2}(X_2)^{-2}_{1/2}$ or $Ir^{3+}(X_2)^{-3}_{1/2}X^{-1.5}$. Another type of charge balance between $Ir^{3+}$ and the anions is found in $IrTe_2$ (*3*). In that case, the tellurium anions form bonds with each other within a tridimensional polymeric network and thus exhibit the $-1.5$ oxidation state. This polymeric structure was also found to be presented by several other transition metal ditellurides (*4*).

Nonstoichiometric $Ir_{1-x}Te_2$ (with $x$ = 0.25, i.e., $Ir_3Te_8$) has been reported as exhibiting a cubic lattice ($a$ = 6.4138(6) Å) (*5*, *6*), the proposed structure being that of pyrite ($FeS_2$) with the expected $Pa3$ space group (*7*). In view of the unforeseen polymeric structure of $IrTe_2$, we considered worthwhile a structural reinvestigation of $Ir_3Te_8$ and an effort to relate its properties to that of other ditellurides.

## II. Experimental

One of the characteristics of iridium chalcogenide (S, Se, Te) preparation lies in the difficulties in obtaining samples with crystals large enough for single crystal radiocrystallography. Several methods were unsuccessfully tried in order to obtain such crystals (in particular with the use of classical transport agents). Only $Ir_3Te_8$ crystals, grown in tellurium baths, proved of the proper size. Powders were first prepared according to Hocking and White (*7*) and then mixed, in a 1/100 weight ratio, with twice distilled tellurium. The mixture was then ground thoroughly to ensure good homogeneity and sealed, under vacuum, in a silica tube. The preparation was heated up to

* To whom correspondence should be addressed.



0022-4596/91 $3.00

TABLE I

$Ir_3Te_8$ POWDER X-RAY DIFFRACTION DIAGRAM, WITH OBSERVED AND CALCULATED $d_{hkl}$ VALUES, AND OBSERVED INTENSITIES

Compound: $Ir_3Te_8$
Crystalline system: cubic
Lattice parameters: $a$ = 6.4113(3) Å
Cell volume: $V$ = 263.54(4) Å$^3$

Powder X-ray diffraction data:

| $h$ | $k$ | $l$ | $d_{obs}$ | $d_{cal}$ | $I/I_0$ | $h$ | $k$ | $l$ | $d_{obs}$ | $d_{cal}$ | $I/I_0$ |
|---|---|---|---|---|---|---|---|---|---|---|---|
| 1 | 0 | 0 | 6.39 | 6.41 | 2 | 4 | 2 | 1 | 1.3986 | 1.3991 | 25 |
| 1 | 1 | 0 | 4.52 | 4.53 | 2 | 3 | 3 | 2 | 1.3670 | 1.3669 | 10 |
| 1 | 1 | 1 | 3.700 | 3.701 | 7 | 4 | 2 | 2 | 1.3090 | 1.3087 | 12 |
| 2 | 0 | 0 | 3.207 | 3.206 | 29 | 3 | 3 | 3 | 1.2338 | 1.2339 | 40 |
| 2 | 1 | 0 | 2.868 | 2.867 | 95 | 4 | 3 | 2 | 1.1903 | 1.1906 | 25 |
| 2 | 1 | 1 | 2.6176 | 2.6174 | 67 | 5 | 2 | 1 | 1.1705 | 1.1705 | 18 |
| 2 | 2 | 0 | 2.2651 | 2.2667 | 27 | 4 | 4 | 0 | 1.1331 | 1.1334 | 22 |
| 3 | 1 | 1 | 1.9335 | 1.9331 | 100 | 5 | 3 | 1 | 1.0838 | 1.0837 | 3 |
| 2 | 2 | 2 | 1.8514 | 1.8508 | 10 | 4 | 4 | 2 | 1.0687 | 1.0686 | 11 |
| 3 | 2 | 0 | 1.7787 | 1.7782 | 19 | 6 | 1 | 0 | 1.0541 | 1.0540 | 10 |
| 3 | 2 | 1 | 1.7144 | 1.7135 | 47 | 5 | 3 | 2 | 1.0402 | 1.0401 | 20 |
| 4 | 0 | 0 | 1.6028 | 1.6028 | 4 | 6 | 2 | 0 | 1.0138 | 1.0137 | 8 |
| 4 | 2 | 0 | 1.4328 | 1.4336 | 21 | | | | | | |

*Note.* $w = 6.30 \times 10^{-4}$. Average $2\theta$ angle deviation = 17/1000. The minimized $w$ factor is: $w = 16/(n_p - n_v) \times ((\sin^2\theta_{cal} - \sin^2\theta_{obs} - D\theta_{ori} \sin^2\theta_{obs})/d\theta \sin 2\theta_{obs}))^2$, where $n_p$ is the number of considered $hkl$ planes and $n_v$ the number of variables. $\theta_{cal}$ and $\theta_{obs}$ are the calculated and observed reflection angles. $d\theta$ is a prefixed angle shift (here equal to 0.03°) whereas $D\theta_{ori}$ is the origin shift (here taken equal to zero). Satisfactory $w$ range generally from $7 \times 10^{-4}$ downward.

1050°C, held at that temperature for 4 hr and then slowly cooled at a rate of 5°C/hr. After cooling to room temperature, the crystals were recovered by sublimation of tellurium at 400°C under static vacuum. A semiquantitative elemental analysis by Energy Dispersive X-ray Analysis (EDAX) revealed a Te/Ir ratio close to the nominal composition $Ir_3Te_8$. The compound, obtained in these conditions, will be referred to as $Ir_3Te_8$, although, from the structural work (vide infra), the iridium content may be somewhat lower ($Ir_{2.915(6)}Te_8$). Various preparations with lower iridium content did not seem to show any composition range, in agreement with previous reports (*5–7*).

The X-ray powder spectra were recorded on a CPS 120 INEL diffractometer (Curved Position Sensitive Detector, Cu$K\alpha_1$ = 1.54059 Å using Si as a standard). The single crystal data collection was made with a CAD4 NONIUS diffractometer (Mo$K\alpha$) and the structure was determined with the SDP-PLUS software package (1985 version) distributed by Enraf–Nonius (*8*).

Magnetic measurements were done on a SETARAM Faraday balance over the temperature range 50–290 K.

## III. X-ray Powder Data Analysis

The indexing and parameter refinement were performed assuming a cubic symmetry with the $a$ parameter of Hocking and White (*7*) and A. Kjekshus *et al.* (*5*). The results were quite satisfactory and led to $a$ = 6.4113(3) Å with a reliability factor of $w = 6.310^{-4}$ (see Table I).

The examination of the various indexed planes shows one reflection ((110)) with a

TABLE II

ANALYTICAL AND CRYSTALLOGRAPHIC DATA PARAMETERS OF THE X-RAY DATA COLLECTION AND REFINEMENT

1. Physical, crystallographic and analytical data
   Formula: $Ir_{2.915(6)}Te_8$ — Molecular weight: 1581.12g
   Color: Black
   Crystal system: Trigonal — Space group: $R$-3 ($n$°148)
   Room temperature crystallographic constants: $a$ = 6.4113(3) Å (pseudo cubic cell)
   Density (calc.): 6.0
   Absorption factor: $\mu$(Mo$\alpha$) = 593.7 $cm^{-1}$
2. Data collection
   Temperature: 273 K
   Radiation: Mo$K\alpha$ — Monochromator: oriented graphite (002)
   Scan mode: $w/2\theta$ — Scan angle: 1.5 + 0.35 tan($\theta$)
   Recording range: 1.5–35°
   Standard reflexions: (14–4), (21–3), (30–4) (every 3600s)
3. Refinement conditions
   Recorded reflexions in a $\frac{1}{8}$ space: 2518
   Independent reflexions: 418
   Refined parameters: 24
   Reliability factors: $R = \Sigma|F_0| - |F_c|/\Sigma|F_0|$
   $R_w = (\Sigma(|F_0| - |F_c|)^2/\Sigma F_0^2)^{1/2}$
   Weighting scheme: pivot point ($F$ = 35) (cut off 2.0)
4. Refinement results
   $R$ = 0.020 $R_w$ = 0.020
   Extinction coefficient: $E_c = 9.08(9).10^{-7}$
   Difference Fourier maximum peak intensity: 3.3(0.7)e/Å$^3$

weak intensity ($I/I_0$ = 2/100) that was not reported in previous work and precludes the pyrite space group $Pa3$. Several subsequent runs confirmed the systematic presence of that reflection line (it is indeed found on the single crystal data as well). This led to five possible space groups for the phase: $P23$, $Pm3$, $P432$, $P$-$43m$, and $Pm3m$. However, these groups were eliminated by Hocking and White because none could fit the observed intensities well enough. Different structure calculations carried out from these five sets of space groups confirmed that fact. Assuming a pyrite-type structure, this result meant that another symmetry had to be chosen. A previous study by A. Kjekshus *et al.* had shown that a rhombohedral symmetry was the only one appropriate for pyrite-type $Rh_3Te_8$. Consequently, the same $R$-3 space group has been chosen for our structure refinement. An analogous distortion was suggested by Squattrito *et al.* for $Ir_{2.7}Se_8$ (*9*). Because there is no observed splitting in the powder diffraction lines, this means that the rhombohedral distortion has no measurable influence on the cubic axis system. This is why only the cubic indexed spectrum is given in Table I.

## IV. Single Crystals Studies and Structure Refinement

Through successive cuttings of a large crystal, a very small crystal fragment was prepared for the X-ray diffraction data collection (see Table II for the parameters used). Because of the heavy absorption coefficient (593.7 $cm^{-1}$), an absorption correction was applied to the data, according to the empirical method of N. Walker and

TABLE III

POSITIONAL PARAMETERS AND THEIR ESTIMATED STANDARD DEVIATIONS

| Atom | $x$ | $y$ | $z$ | $B_{eq}$[a] | $\tau$ | Site |
|---|---|---|---|---|---|---|
| Ir1 | 0.5 | 0.5 | 0 | 0.97(3) | 0.737(1) | 3(e) |
| Ir2 | 0 | 0 | 0 | 0.68(1) | 0.704(3) | 1(a) |
| Te1 | 0.3722(1) | 0.3722(1) | 0.3722(1) | 1.32(1) | | 2(c) |
| Te2 | 0.8724(1) | 0.1273(1) | 0.6276(1) | 1.42(2) | | 6(f) |

[a] Isotropic equivalent thermal parameter defined as: $B_{eq}$ (Å$^2$) = 4/3 $\Sigma_i\Sigma_j\beta_{ij}a_ia_j$.

D. Stuart (*10*) (the lack of thermal anisotropy before any correction and the absence of neat faces for the sample favor the use of such a method). Prior to this correction, the agreement in the averaging of equivalent reflections was 0.030 for the observed and accepted ones and only 0.050 for the observed ones. After absorption correction, these figures dropped to 0.020 and 0.022, respectively. Refinement of the structure in the $R$-3 space group with $Ir_1$ and $Ir_2$ in 3(e) and 1(a) positions and $Te_1$ and $Te_2$ in 2(c) and 6(f) was started, the occupancy ratio of the iridium sites being freed, in accord with a statistical distribution on the octahedral sites. Without absorption correction, and with atomic isotropic factors, $R$ and $R_w$ yielded the values 0.060 and 0.075, whereas with anisotropic factors, one had 0.051 and 0.065. After absorption correction, the figures became 0.030 and 0.041, respectively. Finally, the use of a pivot weighting scheme drove those values down to $R = R_w = 0.020$ (the weighting scheme is such that $w = F/$ pivot if $F <$ pivot and $w =$ pivot$/F$ if $F >$ or $=$ pivot, with a pivot point $F = 35$ and a cut off $= 2.0$) (*8*).

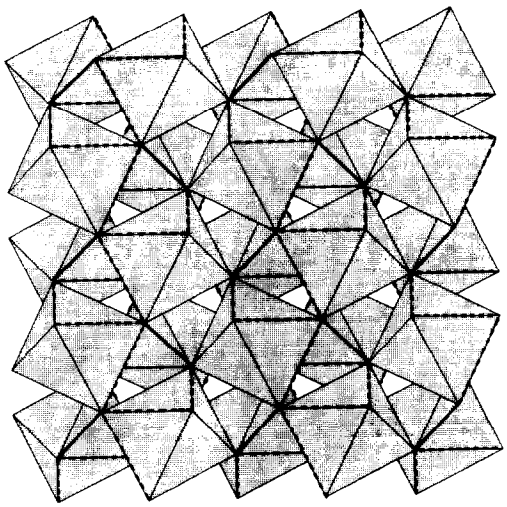

FIG. 1. Representation of octahedra arrangement in $Ir_3Te_8$ in the (001) plane. Dashed lines correspond to Te–Te distances of about 3.57 Å, while thick ones represent Te–Te pairs.

Fractional coordinates and thermal parameters are gathered in Table III and Table IV, respectively. From the occupancy ratio, it can be seen that the phase, within $3\sigma$, may not be stoichiometric since one obtains the composition $Ir_{2.915(6)}Te_8$. The thermal factors have the expected values.

## V. Structure Description

$Ir_3Te_8$ structure is indeed of the pyrite ($FeS_2$) type, with a statistical distribution of

TABLE IV

THERMAL PARAMETERS U (IN Å$^2$)

| Atom | $U_{11}$ | $U_{22}$ | $U_{33}$ | $U_{12}$ | $U_{13}$ | $U_{23}$ |
|---|---|---|---|---|---|---|
| Ir1 | 0.0070(4) | 0.0079(4) | 0.0161(7) | −0.0005(4) | −0.0010(5) | 0.0007(5) |
| Ir2 | 0.0056(3) | $U(1,1)$ | $U(1,1)$ | 0.0004(4) | $U(1,2)$ | $U(1,2)$ |
| Te1 | 0.0111(3) | $U(1,1)$ | $U(1,1)$ | 0.0012(3) | $U(1,2)$ | $U(1,2)$ |
| Te2 | 0.0114(4) | 0.0113(4) | 0.0228(7) | −0.0007(3) | −0.0015(5) | 0.0011(5) |

*Note.* The expression of the general temperature factor is: $\exp(-2\pi^2(U_{11}h^2a^{*2} + U_{22}k^2b^{*2} + U_{33}l^2c^{*2} + 2U_{12}hka^*b^* + 2U_{13}hla^*c^* + 2U_{23}klb^*c^*))$.

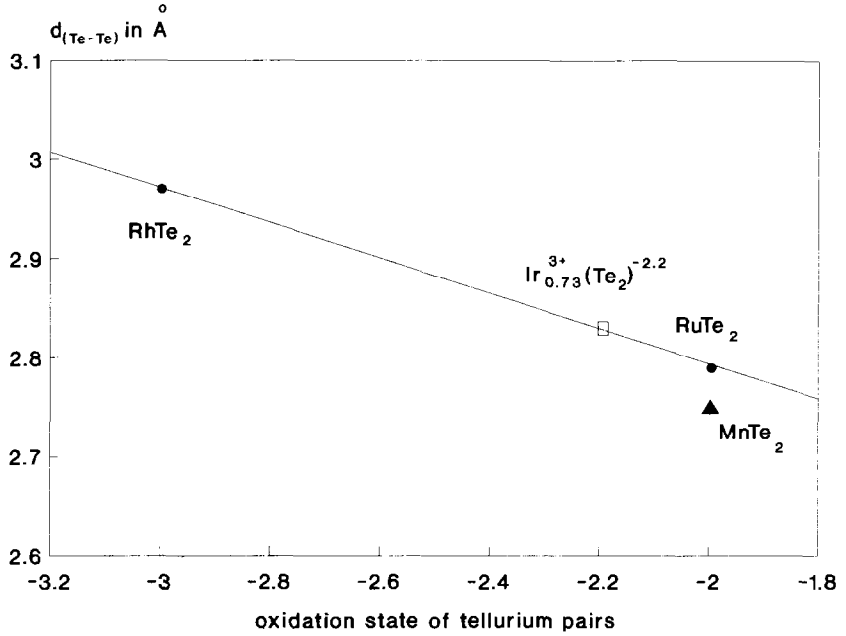


FIG. 2. Variation of the Te–Te bond distance of anionic pairs in accurately and recently studied ditellurides of Rh and Ru, and in $Ir_3Te_8$ (with the proper oxidation state of $-2.2$ per $Te_2$) versus tellurium oxidation state. A straight line goes through the three data points. Note that the triangle representing $MnTe_2$ departs from the line, probably because this phase is the only pure pyrite-type structure, whereas the others present a polymeric modification (see text). $CuTe_2$ as border case was not considered.

Ir atoms on the cationic sites. Each iridium cation is surrounded by a strongly distorted tellurium octahedron, while each anion is engaged in a Te–Te pair and belongs to three adjacent polyhedra as shown in Fig. 1. In each $IrTe_6$ group, the Ir–Te distances are very similar, with a mean bond length of 2.654 Å (see Table V). This result is very close to that obtained in $IrTe_2$, with $d_{Ir-Te}$ = 2.650 Å (*3*). Because we suspected in the present phase an oxidation state of +III and a low spin configuration for the iridium cations as found for the other chalcogenides (see below for the magnetic confirmation), we expect an effective ionic radius (IR) of 0.68 Å (from Shannon's data (*11*)). Using an IR of 2.21 Å for the tellurium anions ($Te^{2-}$) (*11*), a value of 0.44 Å is calculated. This strong discrepancy has been pointed out with all the other iridium dichalcogenides, and we believe that a value of about 0.50 Å for low spin $Ir^{3+}$ should be considered. The still lower value calculated here could be attributed to a higher oxidation state of Te (mean oxidation state = $-1.1$) increasing the actual anionic radius. These conclusions are very well supported by the similar rhodium phases that show a calculated radius of about 0.50 Å (*5*). In addition, with a mean Rh–S distance of 2.365 Å in $Rh_2S_3$ (*12*), the low spin $Rh^{3+}$ IR is calculated at 0.52 Å. Note that this phase includes only $S^{2-}$ ions for which the anionic radius is well known and accepted (isostructural $Ir_2S_3$ with cell parameters quasi-identical to that of the rhodium derivative also exists, but its structure has not been solved).

Looking now at the Te–Te pairs, it was found that their mean bond length is equal to 2.833 Å. Such a distance must be compared

TABLE V

BOND DISTANCES (IN Å) AND ANGLES (IN DEGREES) AROUND EACH METAL TYPE FROM $Ir_3Te_8$ REFINEMENT WITH ESTIMATED STANDARD DEVIATIONS IN PARENTHESES

| | | |
|---|---|---|
| Interatomic distances | | |
| $Ir_1$–$Te_1^{i}$ | 2.6529(6) | ×2 |
| $Ir_1$–$Te_2^{ii}$ | 2.653 (2) | ×2 |
| $Ir_1$–$Te_2^{iii}$ | 2.655 (2) | ×2 |
| $Te_1^{iv}$–$Te_2^{ii}$ | 3.566 (2) | ×2 |
| $Te_1^{iv}$–$Te_2^{iii}$ | 3.571 (2) | ×2 |
| $Te_1^{iv}$–$Te_2^{v}$ | 3.928 (2) | ×2 |
| $Te_1^{iv}$–$Te_2^{vi}$ | 3.926 (2) | ×2 |
| $Te_2^{ii}$–$Te_2^{iii}$ | 3.928 (2) | ×2 |
| $Te_2^{ii}$–$Te_2^{vi}$ | 3.570 (2) | ×2 |
| Angles | | |
| $Te_2^{ii}$–$Ir_1$–$Te_1^{i}$ | 95.53 (4) | ×2 |
| $Te_2^{ii}$–$Ir_1$–$Te_1^{iv}$ | 84.47 (4) | ×2 |
| $Te_2^{iii}$–$Ir_1$–$Te_1^{iv}$ | 84.58 (5) | ×2 |
| $Te_2^{iii}$–$Ir_1$–$Te_1^{i}$ | 95.42 (5) | ×2 |
| $Te_2^{v}$–$Ir_1$–$Te_2^{vi}$ | 95.45 (3) | ×2 |
| $Te_2^{v}$–$Ir_1$–$Te_2^{iii}$ | 84.55 (3) | ×2 |
| Interatomic distances | | |
| $Ir_2$–$Te_2$ | 2.652 (2) | ×6 |
| $Te_2^{iv}$–$Te_2^{vi}$ | 3.923 (3) | ×6 |
| $Te_2^{iv}$–$Te_2^{iii}$ | 3.570 (2) | ×6 |
| Angles | | |
| $Te_2^{i}$–$Ir_2$–$Te_2^{vi}$ | 84.59 (6) | ×6 |
| $Te_2^{i}$–$Ir_2$–$Te_2^{iii}$ | 95.41 (6) | ×6 |
| Interatomic distances between Te of the pairs | | |
| $Te_1$–$Te_1$ | 2.837 (2) | |
| $Te_2$–$Te_2$ | 2.832 (3) | |

*Note.* We define symmetry elements applied to atom positions as (i) x y z, (ii) z x y, (iii) y z x, (iv) −x −y −z, (v) −z −x −y, (vi) −y −z −x.

with $Te_2$ pairs in pyrite-like phases. For instance, in $RuTe_2$ and $MnTe_2$ ($(M^{2+}(Te_2)^{2-}$ charge balance), the Te–Te distances are equal to 2.791 and 2.750 Å, respectively (*13*). These values are significantly lower than that calculated in $Ir_3Te_8$; this may correspond to additional electron concentration on the tellurium pairs in the iridium phase. An evidence of this assumption can be given by the pyrite-like $RhTe_2$ phase in which the increased anionic charge due to the presence of $Rh^{3+}$ leads to a large $d_{Te-Te}$ of 2.969 Å ($(Te_2)^{-3}$) (*5*). Actually, this hypothesis is schematically shown in Fig. 2 where the Te–Te pair distances are plotted versus their oxidation state. Consideration of the actual composition of the iridium telluride ($Ir_{0.73}Te_2$) shows that an oxidation state of −2.2 is to be taken for the $Te_2$ pair ($Ir^{3+}_{0.73}(Te_2)^{-2.2}$). The case of the $Ir_3Te_8$ structure is not however clear if one now considers the distances between the tellurium pairs.

In Table V, the interatomic $Te_2$ pair lengths show two characteristic distances of 3.93 and 3.57 Å. The first corresponds to a simple contact distance (similar to that found in $HfTe_2$ and $ZrTe_2$), whereas the second obviously implies a bonding, as already

TABLE VI

CELL PARAMETERS (IN Å), VOLUME (IN Å$^3$) AND INTERATOMIC DISTANCES (IN Å) IN DITELLURIDES OF TRANSITION ELEMENTS (FROM (*5*) AND (*12*))

| Compound | Parameters | Volume | $d$(M–Te) | $d$(Te–Te) |
|---|---|---|---|---|
| $MnTe_2$ | 6.951 | 335.8 | 2.907 | **2.750** |
| | | | | 3.955 |
| | | | | 4.262 |
| $FeTe_2$[a] | 6.2937 | 249.3 | 2.619 | **2.616** |
| | | | | 3.547 |
| | | | | 3.855 |
| $NiTe_2$[a] | 6.374 | 259.0 | 2.653 | **2.650** |
| | | | | 3.592 |
| | | | | 3.904 |
| $CuTe_2$[a] | 6.6052 | 288.2 | 2.749 | **2.746** |
| | | | | 3.722 |
| | | | | 4.046 |
| $RuTe_2$ | 6.3906 | 261.0 | 2.648 | **2.789** |
| | | | | 3.567 |
| | | | | 3.914 |
| $RhTe_2$ | 6.4481 | 268.1 | 2.659 | **2.969** |
| | | | | 3.560 |
| | | | | 3.951 |
| $OsTe_2$ | 6.3968 | 261.8 | 2.647 | **2.830** |
| | | | | 3.561 |
| | | | | 3.918 |

*Note.* Bold figures relate to the $Te_2$ pair of the structure. $MnTe_2$ is the only pure pyrite type with no inter $Te_2$ bonds (distance of 3.955 Å or more between pairs). $FeTe_2$, $NiTe_2$, $RuTe_2$, $RhTe_2$, and $OsTe_2$ show $Te_2$ weakly bonded pairs (the distances equal about 3.57 Å between tellurium in polymeric $IrTe_2$ (*3*)). $CuTe_2$ is a border case with inter $Te_2$ pairs distance of 3.722 Å between the above length values.

[a] Distances calculated with a classical fractional coordinate $u$ value of 0.38.

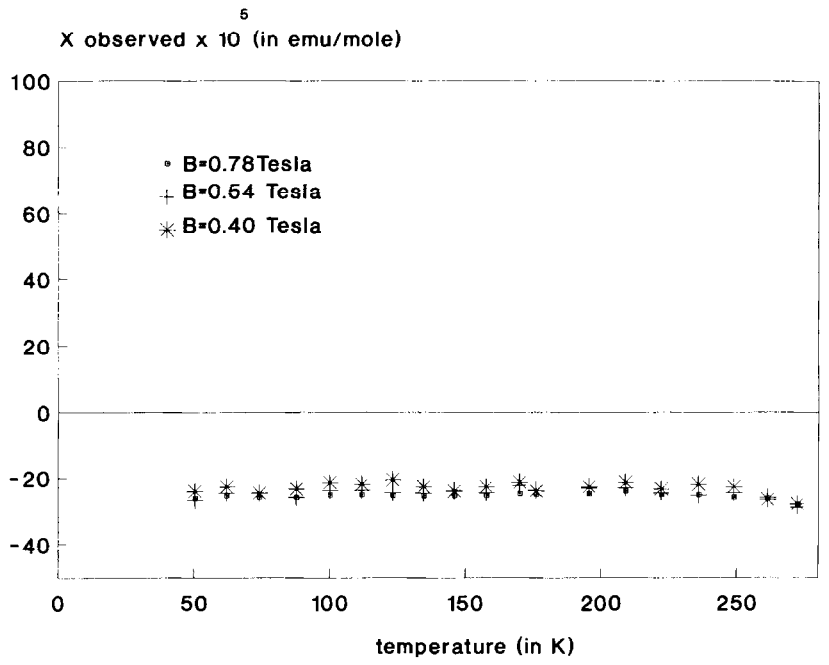


FIG. 3. Variation of the magnetic susceptibility of $Ir_3Te_8$ versus temperature. The diamagnetism observed confirms the $d^6$ low spin configuration of $Ir^{3+}$, with a probable weak underlying Pauli paramagnetism.

mentioned in other examples (*3*, *4*). Since each tellurium of a pair is bonded to two others belonging to the same iridium coordination octahedron, in the way presented in Table V, this means that there exists a polymeric tellurium network within the $Ir_3Te_8$ structure, very much as in polymeric $CdI_2$-like $IrTe_2$. In that phase a distance of 3.53 Å was found to correspond to a bonding interaction through Extended Hückel calculations (*3*). It is to be pointed out that the same Te–Te bonding distances can be found in most ditellurides of transition elements with pyrite-like structures (*5*, *13*). Table VI gathers some cell characteristics and interatomic distances of those phases. All the compounds listed in that table, with the remarkable exception of $MnTe_2$, present a polymeric pyrite-type structure, with very short, medium, and long Te–Te distances, corresponding respectively to pairing, slightly bonding, and nonbonding tellurium atoms. The case of $MnTe_2$ is actually the only one that corresponds to a true pyrite-like phase, as also demonstrated by the large volume jump encountered for the cell (336 $Å^3$ instead of about 260 $Å^3$ for the other polymeric structures). Clearly, and as expected, the anionic bonding is accompanied by a strong volume shrinking.[1] One may also expect an influence of the interpair bonding on the Te–Te pair distances.

[1] Note the large metal–chalcogen distance (2.907 Å) observed in $MnTe_2$. This value is in good agreement with the sum of effective ionic radii only if we consider a $d^5$ high spin configuration of $Mn^{2+}$ ($IR(Mn^{2+}_{hs}) = 0.83$ Å) (*11*). Even with the lack of magnetic susceptibility data, this suggests that $MnTe_2$ would be alone among the $MTe_2$ phases to present a high spin configuration, while the others exhibit a low spin one. This introduces a separation between high and low spin configuration, and interbonded and noninterbonded $Te_2$ pairs.

Within each $CdI_2$-like and pyrite-like structure, one has to distinguish between the well known true $CdI_2$ and pyrite types and their polymeric modifications as shown by $IrTe_2$ and $Ir_3Te_8$. This is one of the common features presented by the two iridium phases, as far as their structure is concerned. Indeed, the question of the peculiar behavior of the manganese derivative remains to be explained, but it is to be noted that we are dealing with a $d^5$ cation, a species known to show peculiar characteristics (see for instance the behavior of $Mn^{2+}$ in the $MPS_3$ series (*14, 15*)).

Magnetic susceptibility measurements of $Ir_3Te_8$ were performed under three different fields (see Fig. 3). They show a diamagnetic behavior, in agreement with a low spin $d^6$ $Ir^{3+}$ cation. The molar susceptibility $\chi_{mes}$ is equal to $-24 \times 10^{-5}$ emu/mole, a value which does not exactly correspond to the sum of the element Pascal constants ($\chi_{Te} = -7 \times 10^{-5}$ and $\chi_{Ir} = -3.5 \times 10^{-5}$ emu/mole). This discrepancy may be linked to some underlying delocalized Pauli paramagnetism.

## VI. Conclusion

The great ability of tellurium, through its extended orbitals, to modulate its oxidation state continuously from $-$II to $-$I by multiple tellurium bonds leads to the formation of polymeric tellurium networks. We thus must distinguish, in the $CdI_2$ and pyrite-types models, two different, although closely related, subgroups. One corresponds to a true model phase, the other one to a polymeric modification. Note that the polymeric configuration appears only with transition element ions with more than five *d*-electrons. More work is necessary to understand why, in the $MX_2$ family, $MnTe_2$ presents the only genuine pyrite structure, whereas $CuTe_2$ is an interesting, and indeed expected, border case.

## References


1. L. B. Baricelli, *Acta Crystallogr.* **11,** 75 (1958).
2. S. Jobic, P. Deniard, R. Brec, J. Rouxel, M. G. B. Drew, and W. S. F. David, *J. Solid State Chem.* **89,** 315 (1990).
3. S. Jobic, P. Deniard, R. Brec, J. Rouxel, A. Jouanneaux, and A. N. Fitch, *Z. Anorg. Chem.*, to be published.
4. S. Jobic, *et al.*, submitted.
5. A. Kjekshus, T. Rakke, and A. F. Andresen, *Acta Chem. Scand., Ser. A* **32,** 209 (1978).
6. A. Kjekshus, T. Rakke, and A. F. Andresen, *Acta Chem. Scand., Ser. A* **33,** 719 (1979).
7. E. F. Hocking, and J. G. White, *J. Phys. Chem.* **64,** 1042, (1960).
8. P. Frenz, "SDP-PLUS," Enraf–Nonius (1985).
9. P. J. Squattrito, H. You, and J. A. Ibers, *Mater. Res. Bull.* **22,** 75 (1987).
10. N. Walker and D. Stuart, *Acta Crystallogr., Sect. A: Found. Crystallogr.* **39,** 159 (1983).
11. R. D. Shannon, *Acta Crystallogr., Sect. A: Cryst. Phys. Diffr. Theor. Gen. Crystallogr.* **32,** 751 (1976).
12. E. Parthé, D. Hohnke, and F. Hulliger, *Acta Crystallogr.* **23,** 832 (1967).
13. C. Brostigen, and A. Kjekshus, *Acta Chem. Scand.* **24,** 2993 (1970).
14. R. Brec, *Solid State Ionics* **22,** 3 (1986).
15. M. Barf, G. Lucazeau, G. Ouvrard, and R. Brec, *Eur. J. Solid State Inorg. Chem.* **25,** 449 (1988).